Int. J. Electrochem. Sci., 16 **(2021)** Article ID: 21084, doi: 10.20964/2021.08.04

International Journal of
ELECTROCHEMICAL
SCIENCE
www.electrochemsci.org

Ultrasensitive Determination of Dopamine and Uric Acid Based on Gold Nanoparticles@Carbon Dots/Electrochemical Reduced Graphene Oxide modified glassy carbon electrode

Muyi Li, Xiang Yang, Wenjun Liu, Huixian Wang, Hongmei Jiang[*], *Xiaoying Liu*[*]

School of Chemistry and Materials Science, Hunan Agricultural University, Changsha 410128, P.R. China.
[*]E-mail: jhmndcn@hunau.edu.cn (H. Jiang), xyliu@hunau.edu.cn, xiaoyingliu@126.com (X. Liu)

Received: 14 March 2021 / *Accepted:* 13 May 2021 / *Published:* 30 June 2021

An ultrasensitive electrochemical sensing platform based on a glassy carbon electrode (GCE) modified with electrochemically reduced graphene oxide (erGO) and gold nanoparticles@carbon dots (GNPs@CDs) was developed. The hydroxyl-rich CDs were electrochemically synthesized, and the GNPs@CDs were obtained by reducing chloroauric acid with hydroxyl-rich CDs. The electrochemical behavior of the fabricated electrode, GNPs@CDs/erGO/GCE, was explored by cyclic voltammetry and electrochemical impedance spectroscopy. The electrochemical performance of the electrode demonstrated a remarkable enhancement in the peak current toward oxidation of dopamine (DA) and uric acid (UA) with a peak potential separation of 0.15 V in the presence of ascorbic acid (AA). Under optimized conditions, the simultaneous determination of DA and UA was investigated using differential pulse voltammetry (DPV) resulting in a linear response in the concentration ranges of 0.01−5.0 μM and 5.0−20.0 μM for DA and of 0.1−20.0 μM and 20.0−50.0 μM for UA and in a sensitivity of 11.96 and 6.48 μA μM^{-1}, respectively. The prepared electrode also demonstrated long-term stability and good reproducibility and was successfully used for the determination of DA and UA in human serum samples with favorable recoveries.

Keywords: GNPs@CDs/erGO nanocomposite; electrochemical synthesis; simultaneous determination; dopamine; uric acid.

1. INTRODUCTION

Dopamine (DA) and uric acid (UA) are small biomolecules widely distributed in the human body. DA plays an important role in the central nervous system [1], and abnormal DA concentrations can cause diseases such as Parkinson's disease [2]. The concentration of UA reflects the metabolic state of the human body. High concentrations of UA cause an increase in the acidity levels of body fluids and can result in diseases such as gout [3]. Analytical electrochemical methods show some

remarkable advantages like low detection limits, fast analytical speed, low cost, simple operation, and real-time analysis [4]. However, the oxidation of DA and UA on bare electrodes requires a high potential, and the separation of the two oxidation peaks on the bare electrode is impeded by the small difference between the oxidation peak potentials of these two compounds, which greatly reduces the detection efficiency. Furthermore, the presence of ascorbic acid (AA) negatively influences the electrochemical determination of DA and UA. Therefore, choosing suitable electrode modification materials for constructing electrochemical sensors for simultaneous detection of DA and UA would be a significant progress in analytical methods for both clinical and scientific fields [5].

Reduced graphene oxide (rGO) is a reduction product of GO and exhibits a stable structure, which can prevent GO from deteriorating due to chemical reactions [6]. The material is further characterized by a high specific surface area, high chemical stability, and unique electronic and mechanical properties, which has attracted considerable attention in the field of electrochemical sensing [7-10]. At present, the methods of preparing rGO from GO include thermal reduction, chemical reduction, and electrochemical reduction [11]. In recent years, electrochemical reduction methods that require the use of other reagents to enable analysis at mild reaction conditions have been widely employed.

Carbon dots (CDs) were first discovered by Xu et al. in 2004 [12]. In 2006, Sun et al. [13] prepared fluorescent carbon particles with a very wide luminescence range by laser ablation of graphite, which has received the attention of many researchers. CDs possess good catalytic performance and many active functional groups on the surface [14]. In the first reported use of CDs for electrochemical sensing, Zhang combined the surface functional groups of the CDs with the functional groups of the analyte to generate an electric current. However, the oxygen functional groups on the surface of the CDs hindered the transfer of electrons and CDs easily fell off the electrode surface [15]. According to published reports, gold nanoparticles (GNPs) with larger surface areas exhibit excellent electrical conductivity and catalytic activity and have been successfully used as support materials, catalysts, and conductors to amplify nanoparticles for electrochemical reactions [16]. Some reports indicate that the reduced CDs can be synthesized by a one-step electrochemical method [17], and Au ions can be reduced to GNPs in situ. Compared with CDs or GNPs, the formed gold-CDs nanohybrid (GNPs@CDs) demonstrates higher catalytic activity [18, 19], excellent electrochemical behavior [20, 21], and enhanced biocompatibility [22].

In this work, CDs were synthesized by an electrochemical method and then used as reductant and stabilizer to prepare GNPs@CDs. The nanohybrid GNPs@CDs/erGO-modified glassy carbon electrode (GCE) was obtained by one-step electrochemical reduction in a dispersion containing GO and GNPs@CDs. The modified electrode exhibited excellent electrocatalytic properties toward oxidation of DA and UA in the presence of AA, which could be attributed to abundant surface functional groups, a high amount of surface defects, significantly increased specific surface area, and a synergistic catalytic effect between GNPs@CDs and erGO. Due to these properties, an ultrasensitive electrochemical sensing platform based on GNPs@CDs/erGO/GCE was proposed for the simultaneous determination of DA and UA in real samples.

2. MATERIALS AND METHODS

2.1. Chemicals and Solutions

Chloroauric acid ($HAuCl_4 \cdot 4H_2O$) was purchased from Sinopharm Chemical Reagent Co., Ltd. (Shanghai, China). Graphene oxide (GO) was provided by XFNANO Co., Ltd. (Nanjing, China). Dopamine (DA), uric acid (UA), ascorbic acid (AA), and ethylene glycol (EG) were purchased from Aladdin Reagent Co., Ltd. (Shanghai, China). All chemicals were of analytical grade and used directly. The human serum samples were obtained from Hospital of Hunan Normal University (Changsha, China). A stock solution (0.1 M) of DA, UA, and AA was prepared by dissolving appropriate amounts of DA, UA, and AA in 1 mL deionized water. Then, by diluting the stock solution with appropriate amounts of 0.2 M phosphate-buffered saline (PBS), a series of standard solutions of lower concentrations were obtained. Deionized water was used in all experiments.

2.2. Apparatus

All electrochemical measurements including cyclic voltammetry (CV), differential pulse voltammetry (DPV), and electrochemical impedance spectroscopy (EIS) were performed on a CHI 660E electrochemical workstation (Shanghai Chenhua Instrument Co., Ltd., China). An UV-visible spectrophotometer (Hitachi UV-2600) was used to measure the UV-visible absorption spectrum of CDs, GNPs@CDs, GO, and GNPs@CDs/GO. The surface morphology and element distribution via energy dispersive X-ray spectroscopy (EDS) of CDs, GNPs@CDs, and GNPs@CDs/GO were studied by a transmission electron microscopy (TEM, FEI Tecnai G2 F20, USA). X-ray photoelectron spectroscopy (XPS, Thermo Scientific K-Alpha 1063, USA) was used to analyze the elemental composition of CDs and GNPs@CDs. A digital precision pH meter (Leici Instruments, Shanghai, China) was used to measure the pH of the solutions.

2.3. Synthesis of CDs and GNPs@CDs

CDs were synthesized by an electrochemical method published previously (Scheme 1). In short, 0.2 M NaOH was added to 5 mL deionized water and then thoroughly mixed with 30 mL ethylene glycol. After electrolysis under DC power for 40 min, the mixture was passed through a 0.45-micron filter membrane and poured into a trap in a dialysis bag with molecular-weight cutoff of 1,000 Da, after which dialysis was performed for 48 h [17]. Finally, the obtained CD dispersion solution was dried under vacuum to obtain a CD solid for further use. As a result of optimizing the ratio of CD to chloroauric acid, 0.1 mg mL^{-1} CDs and 0.2 mM chloroauric acid were typically added to 1 mL deionized water and reacted for 2 h [18]. The obtained orange-red mixture of GNPs@CDs was stored at 4 ℃ before use.

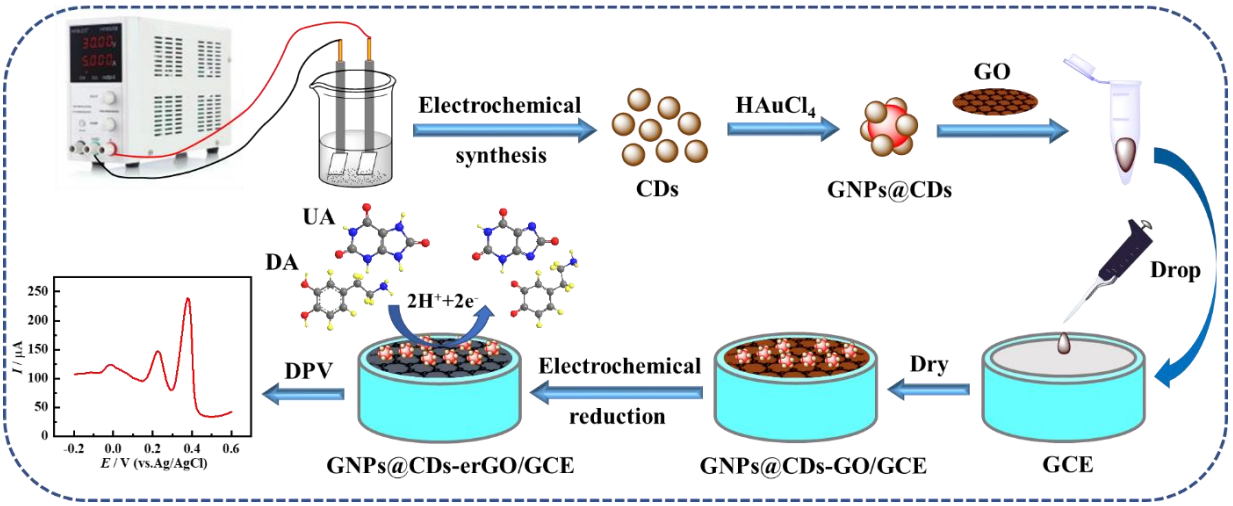

Scheme 1. The schematic illustration of the synthesis of GNPs@CDs/erGO and of the possible mechanism for electrochemical sensing of DA and UA at the GNPs@CDs/erGO/GCE.

2.4. Fabrication of GNPs@CDs/erGO/GCE

Firstly, 200 μL of the above-mentioned GNPs@CDs mixture and 80 μL of a 2 mg mL^{-1} GO mixture were dispersed in 1 mL 0.2 M PBS (pH=7.0) under ultrasonic treatment for 30 min to form a GNPs@CDs/GO dispersion.

The bare GCE was carefully polished into a mirror-like appearance with a fine alumina slurry with particle diameters of 0.3 μm and 0.05 μm. Then, the polished GCE was washed several times alternately with anhydrous ethanol and deionized water, and the glassy carbon surface was blown dry with high-purity nitrogen. The GNPs@CDs/GO/GCE was prepared by a simple drop casting method. More specifically, 5 μL of the GNPs@CDs/GO dispersion were carefully dropped and coated on the surface of the GCE with a micropipette and then dried with an infrared lamp, before 2 μL of 0.05% Nafion was added dropwise followed by drying with an infrared lamp to form a sensing membrane. Then, the prepared electrode was scanned for 10 cycles from -1.5 to 0 V in 0.2 M PBS at pH=7.0 at a sweep speed of 50 mVs^{-1} to effect the electrochemical reduction of graphene oxide and obtain GNPs@CDs-erGO/GCE.

2.5. Electrochemical Measurements

CV and EIS were performed in 0.1 M KCl containing 5 mM $[Fe(CN)_6]^{3-/4-}$ as a redox probe solution. EIS was measured over a frequency range of 100 kHz to 0.01 Hz. The CV electrochemical response of different electrodes was measured to the standard solution of 20 μM DA, 20 μM UA, and 1.6 mM AA. DPV was employed to detect DA and UA. A conventional three-electrode assembly was used for electrochemical measurement and detection in a 10 mL electrochemical cell. The system employed bare or modified GCE as the working electrode, Ag/AgCl electrode as the reference electrode, and platinum as the counter electrode. The wire served as an auxiliary electrode. To increase the response peak current, an appropriate accumulation time was applied before the CV and DPV

measurements. DPV used a voltage range of -0.2 V to 0.6 V, a step potential of 4 mV, an amplitude of 50 mV, a pulse width of 0.06 s, and a pulse period of 0.5 s. Unless otherwise stated, 0.2 M PBS was used as the supporting electrolyte. All measurements were performed at room temperature.

3. RESULTS AND DISCUSSION

3.1. Material characterization

According to TEM images, the average particle size of CDs is 1.84 ± 0.39 nm (Figure 1A, S1A). The high-resolution TEM (HRTEM) images of single CDs indicate typical lattice spacings of 0.21 nm and 0.32 nm corresponding to the in-plane lattice spacing of graphene (100 faces) and the spacing between graphene layers (002 faces) (Figure 1A).

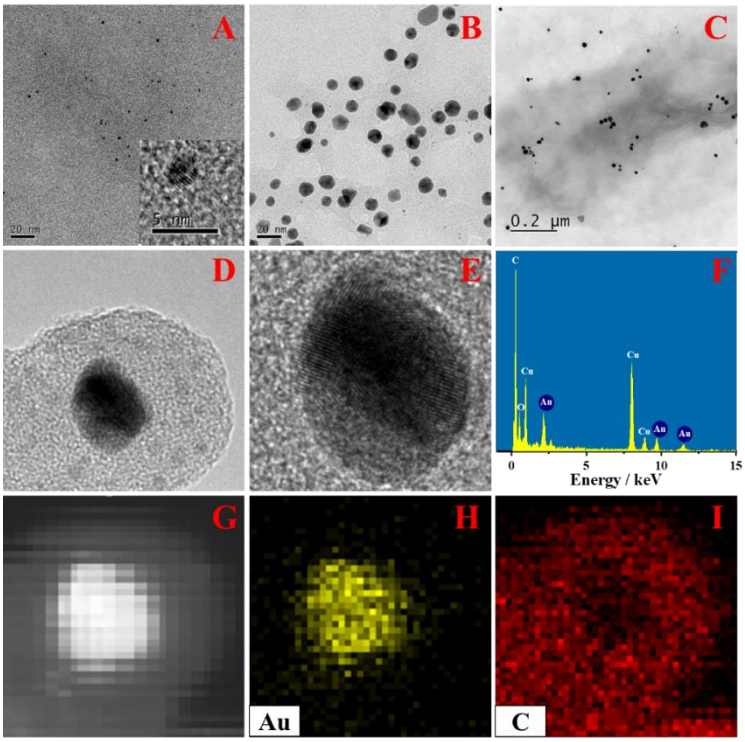

Figure 1. TEM of (A) CDs, (B) and (D) GNPs@CDs, and (C) GNPs@CDs/GO; (E) HRTEM of GNPs@CDs; (F) EDS of GNPs@CDs; (G) HAADF-STEM images, and STEM-EDS elemental map of GNPs@CDs of (H) Au and (I) C element.

This result confirms previous reports on CDs. Figure 1 (B, D) shows TEM images of GNPs successfully reduced by using CDs prepared by ethylene glycol as reducing agents with an average particle size of 10.79 ± 1.55 nm (Figure S1B). According to the TEM of GNPs@CDs/GO composites, graphene was distributed in a more uniform plate shape, and gold nanoparticles were well dispersed among GO (Figure 1C). As a result, GNPs@CDs hybrids were formed. Figure 1E shows the HRTEM

lattice fringes of GNPs with a lattice spacing of 0.22 nm and 0.20 nm, corresponding to the Au (111) and Au (002) planes [23]. In addition, CDs are observed on the (111) crystal planes of GNPs in the HRTEM lattice image of GNPs@CDs (Figure 1E). Lattice fringes with GNPs@CDs also confirm the existence of different crystal planes for graphitic carbon and gold crystals. The STEM-EDS elemental maps of the synthesized GNPs@CDs nanoparticles are shown in Figure 1F and 1G, in which the brighter spots are assigned to GNPs due to their higher atomic number compared to CD nanoparticles [24]. The EDS mapping and the line scan of GNPs@CDs indicate the positions of Au and C (Figures 1H and 1I) and that the carbon element is wrapped around the gold particles, which proves the successful synthesis of GNPs@CDs.

XPS was performed to further characterize the chemical composition of CDs and GNPs@CDs nanocomposites, and the survey spectra and deconvoluted spectra are shown in Figure 2. The wide-scan XPS spectrum of CDs in Figure 2A confirms the presence of both carbon and oxygen. Figure 2C confirms the presence of gold in addition to carbon and oxygen in the GNPs@CDs nanocomposite. The high-resolution Au 4f XPS spectrum in Figure 2E presents two doublet peaks at 83.8 eV and 87.5 eV for Au 4f7/2 and Au 4f5/2, respectively. In this work, GNPs exhibit a negative shift of about 0.2 eV compared to the binding energy of metallic gold (84.1 eV), which can be attributed to the strong interaction between GNPs and CDs [25]. As evident from the high-resolution carbon peaks in CDs and GNPs@CDs, the ratio of the C-C, C-OH, C=O, and COOH peak areas does not change significantly before and after reduction of gold. The ratios of the C-OH peak area after reduction of gold to the peak areas of C=O and COOH are according to expectations (Tabel S1) [26].

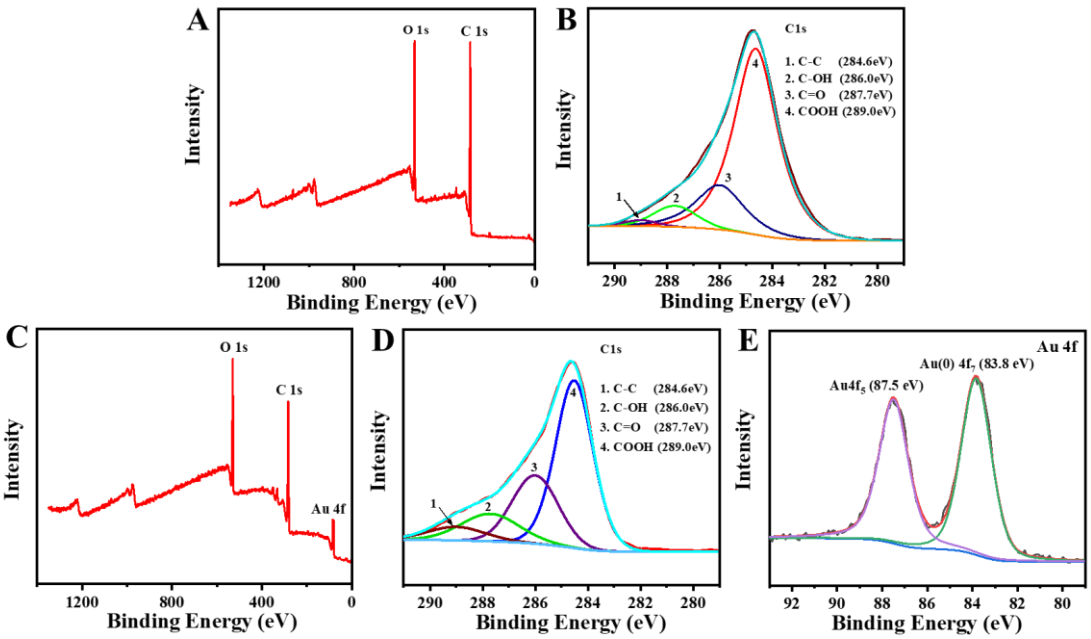

Figure 2. XPS spectra: XPS survey spectrum of (A) CDs and (C) GNPs@CDs nanocomposites; C 1s XPS spectrum of (B) CDs and (D) GNPs@CDs; (E) Au 4f XPS spectrum of GNPs@CDs [26].

After the reduction, the peak area ratio of C-OH to C=O and COOH peaks decreased, indicating the reduction of chloroauric acid to gold nanoparticles on the surface of the CDs by the hydroxyl groups.

As shown in Figure S2, the surface functional groups at CDs and GNPs@CDs were detected by infrared (IR) spectroscopy. In the IR spectrum, the stretching vibration of C≡C is located at 2351 cm^{-1}, the stretching vibration of C=O is observed at approximately 1632 cm^{-1}, the peak at 1392 cm^{-1} is attributed to C-H, and the antisymmetric vibration of the phenolic hydroxyl group is observed at 1118 cm^{-1}. The peak at 1118 cm^{-1} is less intense on GNPs@CDs than on CDs, which corroborates the reduction effect of the hydroxyl groups on the surface of the CDs.

The UV spectra of CDs, GNPs@CDs, and GNPs@CDs/GO are shown in Figure S2B. The well-defined UV absorption of CDs at 263 nm is attributed to the π-π transition of aromatic compounds, which corresponds to the findings of the IR investigation. In addition to the absorption peak of π-π transition at 263 nm, the spectrum of GNPs@CDs also includes an absorption peak of gold nanoparticles at 529 nm, which confirms the formation of gold nanoparticles through reduction with CDs. The π-π* transition peak of graphene at 235 nm can only be observed in the GNPs@CDs/GO composite, indicating that GNPs@CDs have been anchored on graphene [17].

3.2. Electrochemical properties of modified electrodes

The electrochemical performance of different modified GCEs in 5.0 mM $[Fe(CN)_6]^{3-/4-}$ probe solution was investigated by CV. The corresponding CV curves are plotted in Figure S2C. A pair of redox peaks is observed on the bare GCE, and the difference between the peak potentials of oxidation and reduction (ΔE_p) of 0.09 V indicates a good electron transfer on the bare electrode. Since rGO has a good electron transfer rate, its peak current will be higher than that of a bare electrode. However, the redox peak current of CDs/erGO/GCE is lower than erGO/GCE, because CDs are distributed on the surface of erGO due to π-π conjugation; furthermore, the surface is rich in oxygen-containing functional groups with the ability to accept or lose electrons, which will hinder the transfer of electrons [27]. The GNPs@CDs exhibit higher catalytic activity, excellent electrochemical behavior, and enhanced biocompatibility in comparison to CDs or GNPs. Only the simultaneous addition of CDs and GNPs can synergistically increase the electrode electron transfer rate (Figure S2C) [28]. As expected, GNPs@CDs/erGO/GCE shows excellent electrochemical performance with the highest redox current peak (I_{pa} = 147.45 μA, I_{pc} = 141.8 μA) due to the synergy between GNPs@CDs and GO nanosheets.

EIS is a valuable tool for obtaining interface characteristics and has been widely used for the characterization of various electrochemical sensors [29-32]. Figure S2D shows the Nyquist diagrams of bare GCE, erGO/GCE, CDs/erGO/GCE, and GNPs@CDs/erGO/GCE as well as the electron transfer kinetics and diffusion characteristics. The diameter of the semicircle represents the charge transfer resistance (R_{ct}). The addition of CDs introduces a part of the hydroxyl functional groups, which affects the electron transfer rate on the surface of the rGO; the largest semicircle diameter (297 Ω) obtained for CDs/erGO/GCE indicates that the surface functional groups of CDs hinder the electron transfer process. Compared with the bare GCE (95 Ω), the R_{ct} value of erGO/GCE is close to zero,

which indicates the good conductivity of erGO. A R_{ct} value (113 Ω) similar to the bare electrode is obtained for GNPs@CDs/erGO/GCE, since the surfaces of erGO and GNPs@CDs contain many electrocatalytically active sites, which causes faster redox kinetics. The results demonstrate that GNPs@CDs/erGO nanocomposites can effectively reduce R_{ct}. The conclusion is consistent with that obtained from the probe characterization and proves the accuracy of the result.

3.3. Electrochemical behaviors of DA and UA at modified electrodes

Electrochemical responses of 20 μM DA, 20 μM UA, and 1.6 mM AA were recorded on different electrodes by CV in 0.2 M PBS (pH=6.0). As shown in Figure 3 the degree of separation of DA and UA peaks differs for different electrode pairs. With the bare GCE, the presence of only one broad oxidation peak implies that the current peaks of the three substrates could not be separated. After reducing GO to erGO, the conductivity is significantly improved, and three oxidation peaks can be observed. GO with a large specific surface area can provide abundant adsorption sites for the target analyte, thereby enhancing the electrochemical response signal, so that the three substrates can show high-resolution oxidation peaks at different potentials. However, the sensitivity of the electrochemical response of DA and UA at erGO/GCE was still insufficient. Using the CDs/erGO/GCE resulted in a slight by noticeable improvement. The surface functional groups of CDs may hinder electron transfer, but due to the π-π conjugation between CDs and erGO, the specific surface area of rGO is increased, and more active sites are generated, which increases the response to the substrate [31]. The Zeta potential was used to determine the electronegativity of CDs and GNPs@CDs (Figure S6).

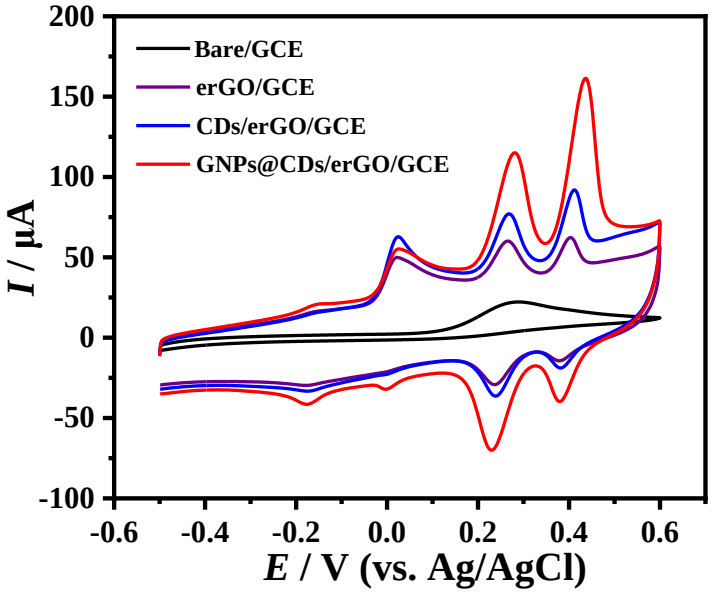

Figure 3. CV current response of differently modified electrodes in 0.2 M PBS (pH 6.0) containing 20 μM DA, 20 μM UA, and 1.6 mM AA at a scan rate of 50 mV s^{-1}.

The result shows that both surfaces are negatively charged and that GNPs@CDs is more negatively charged than CDs, which implies that the nanocomposites exhibit a good electrochemical response toward the positively charged DA and UA. Among the electrodes, GNPs@CDs/erGO nanocomposites demonstrated a significant electrocatalytic activity for the electrochemical oxidation of DA and UA. The addition of electrocatalytically active metal particles further improves the conductivity of the composite material and also increases the surface area of the rGO and the electron transfer rate. Compared with the bare electrode, the response of GNPs@CDs/erGO/GCE to DA and UA can not only separate the three substrate peaks but also increase the sensitivity significantly, which is seldom reported in the previous literature [32, 33].

3.4. Influence of pH

The pH is an important parameter that affects electrochemical reactions directly. The DPV spectra of 10 μM DA and 10 μM UA at different pH are shown in Figure S3A. It is worth noting that the anode peak shifts toward lower values with increasing pH value. The effect of pH on the DA and UA response peak current is shown in Figure S3A and S3C. The anodic peak current increases when increasing the pH from 4 to 6 and gradually decreases with a further pH increase from 6 to 8. The highest response anodic peak current is obtained at pH 6.0. In addition, the anodic peak potential decreases linearly with increasing pH (Figure S3B, S3D). The linear relationship between the peak potential and pH can be expressed as follows：

DA: E_p = -0.063 pH + 0.601 (R^2 = 0.997)

UA: E_p = -0.070 pH + 0.817 (R^2 = 0.999)

The slope of the linear relationship in the figure is very close to the theoretical value of the Nernst equation (59 mV pH^{-1}), indicating that protons (H^+) and electrons (e^-) participate in the electrooxidation process of DA and UA, which is consistent with previous work.

3.5. Influence of scan rate

To provide a deeper insight into the mechanism of electrochemical oxidation, the GCE was used to record the cyclic voltammograms of 10 μM DA and 10 μM UA at various scan rates. Referring to the CV plots in Figure S4, it is worth noting that the redox peak increased with increasing scan rate. At the same time, the background current also increased, probably because a high scan rate would increase the charging current of the double layer. In addition, as the scan rate increased, the anodic peak currents of DA and UA increased and the cathodic peak currents decreased. As shown in Figure S4C and S4D, the anodic and cathodic peak currents of DA and UA are linearly correlated with the scan rate (v, mV s^{-1}), indicating that the electrooxidation of DA and UA is an adsorption-controlled process. The linear regression equations are as follows:

DA: I_{pa} = 0.438v + 10.68 (R^2=0.9948), I_{pc} = -0.550v − 1.84 (R^2 = 0.9935);

UA: I_{pa} = 0.521v + 5.59 (R^2=0.9941), I_{pc} = -0.361v + 8.58 (R^2 = 0.9956).

The electrochemical oxidation of both DA and UA involves the abstraction of two protons under uptake of two electrons (Scheme 1).

3.6. Determination of DA and UA

In the potential range of -0.2 ~ 0.6 V in 0.2 M PBS (pH = 6.0), DPV was used for the determination of DA and UA, which showed high current sensitivity and good resolution (Figure 4). Figure 4A shows the DPV spectrum at different DA concentrations in the presence of 10 μM UA under optimized conditions. The oxidation of DA and UA corresponds to two different oxidation peaks at 299 and 421 mV, respectively. The anodic peak current of DA increased linearly with the increase of DA concentration, while the peak current of UA remained basically unchanged. These results indicate that the change in the concentration of one compound had no significant effect on the peak current of the other compound, indicating that the response of DA and UA to the prepared GNPs@CDs/erGO/GCE was relatively independent. Figure 4B shows the plot of anodic peak current over DA concentration with two linear sections of different slopes.

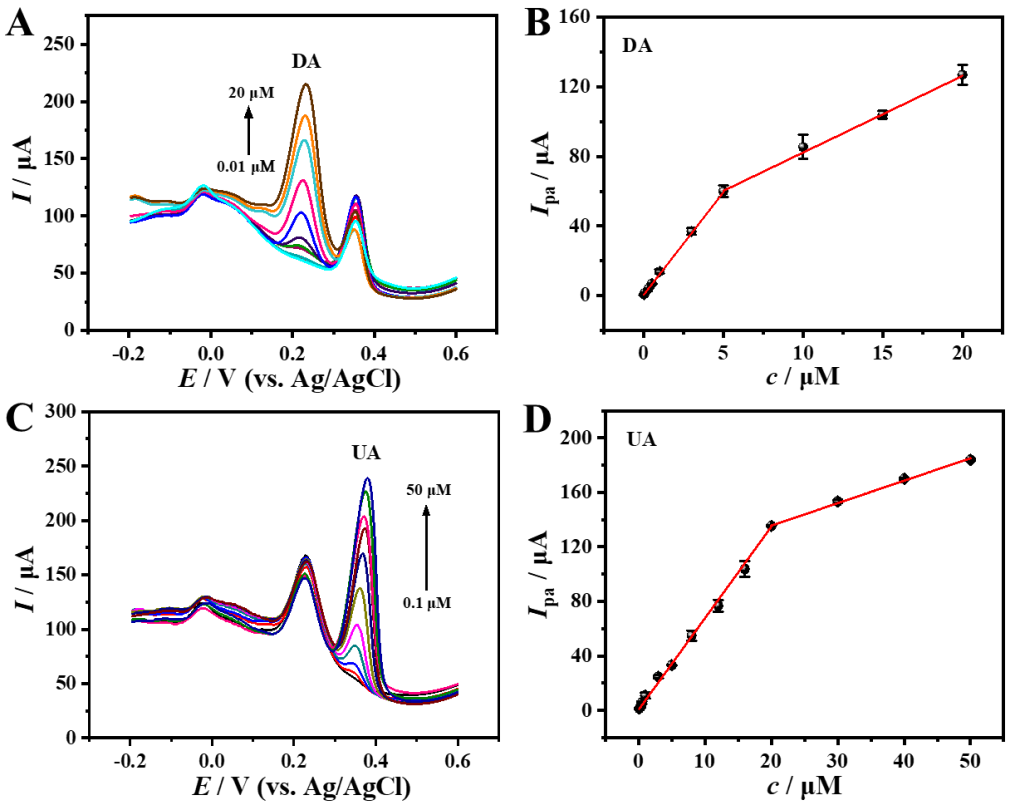

Figure 4. Current responses obtained from DPV measurements using GCE in 0.2 M PBS and 0.1 mM KCl (pH 6.0) with increasing concentrations of (A) DA, (C) UA and the calibration curve of the current versus (B) DA and (D) UA concentrations by DPV measurement.

In the DA concentration range of 0.01 ~ 5.0 μM and 5.0~20.0 μM, the regression equations are I_{pa1}(μA) = 11.92c_{DA}(μM) − 29.76, R^2 = 0.9994, and I_{pa2}(μA) = 4.392c_{DA}(μM) + 25.66, R^2=0.9968, respectively. Referring to Figures 4C and D, the peak oxidation current of UA displays a similar behavior compared to DA and increases linearly in two regimes with the increase of UA concentration in 0.2 M PBS (pH 6.0) containing 10 μM DA. For the UA concentration range from 0.1 to 15.0 μM and from 20.0 to 50.0 μM, the regression equation are determined as I_{pa1}(μA) = 6.48c_{UA}(μM) + 2.36, R^2=0.9969, and I_{pa2}(μA) = 1.66c_{UA}(μM) + 88.91, R^2 = 0.9934, respectively. The analysis characteristics of the DA and UA detection methods of the present study were compared with other reported electrochemical sensors. The main parameters are summarized in Table 1. It is evident that the proposed method exhibited a relatively low limit of detection (LOD) and ultra-high sensitivity compared with similar sensors published in literature. Although the detection range is not optimal, the measurement is more accurate in the lower concentration range, which is more suitable for the measurement with this electrode in complex, real serum samples.

3.7. Stability, reproducibility, and interference studies

To study the stability and reproducibility of the GNPs@CDs/erGO/GCE, five independently fabricated electrodes were employed at a fixed concentration of 10 μM DA and 10 μM UA in 0.2 M PBS (pH 6.0), and the corresponding ampere diagrams were recorded. The results indicated good repeatability and repeatability of the modified electrodes with relative standard deviations of 4.09% and 2.10%, respectively. In addition, the stability of GNPs@CDs/erGO/GCE after 15 cycles of the ampere current was investigated, which did not result in any significant change in the current response. In addition, the anti-interference property of the electrode was studied by adding organic compounds to a concentration of 0.1 mM (urea, ascorbic acid, glucose, L-cysteine, citric acid) and inorganic ions to a concentration of 1 mM ($ZnSO_4$, $CaCl_2$, Na_2CO_3, $NaNO_3$) to 0.2 M PBS (pH 6.0) containing 1.0 μM DA and 1.0 μM UA (Figure S5). Compared to the samples containing the analytes only, the current responses did not show noticeable changes. The results confirm that the developed electrode shows excellent selectivity for DA and UA molecules.

Table 1. Comparison of the analytical performance characteristics of the proposed DA and UA sensor with other existing composite sensors.

Electrode	Analytical technique	Detection Range (μM)		LOD (μM)		Sensitivity (μA μM^{-1})		Reference
		DA	UA	DA	UA	DA	UA	
Fc-S-Au/C NC/graphene/GCE	DPV	0.2-2.5 2.5-97.5	0.6-9.2 9.2-273	0.05	0.12	0.6174 0.0596	0.1105 0.0151	[28]
Au/Fe_3O_4/GCE	i-t	0-0.8	−	0.0027	−	0.034	−	[34]
d-Fe_2O_3/GO/GCE	DPV	10-100	10-100	0.0032	0.0025	0.1062	0.0186	[35]
Au_1Pt_2NPs/S-NS-GR/GCE	DPV	0.01-400	1-1000	0.006	0.038	0.1956	0.0326	[36]
Graphene-AuNPs/GCE	DPV	5.0-1000	−	1.9	−	0.036	−	[37]

OPPy/ERGO/GCE	DPV	2.0-160	–	0.5	–	0.33	–	[32]
TiN-rGO/GCE	DPV	5-175	30-215	0.159	0.350	0.016	0.007	[38]
ERGO-PEBT/AuNPs/GCE	DPV	0.5-20	2-70	0.009	0.046	0.09	0.023	[33]
p-GLY/GO/GCE	DPV	0.2-62	0.10-105	0.011	0.061	0.534	0.103	[39]
β-CD/CQDs/GCE	DPV	4-220	0.3-200	0.14	0.01	0.288	0.239	[40]
Cubic Pd/RGO/GCE	DPV	0.45-421	4-469.5	0.18	1.6	0.0627	0.019	[41]
Au@Pd HNRs/BG/GCE	DPV	50.00-275.00	–	4.58	–	0.005		[42]
RGO/PDA/Au/GCE	DPV	340-610	380-2680	110	130	0.069	0.011	[43]
GNPs@CDs/erGO/GCE	DPV	0.01-5 5-20	0.1-20 20-50	0.0031	0.0335	11.96 4.39	6.48 1.66	This Work

DA and UA are present in most biological fluids. To verify the applicability of the developed sensor to samples from such fluids, GNPs@CDs/erGO/GCE was employed to determine the concentration of DA and UA in human serum samples. The samples were diluted by a factor of 500. In addition, DA and UA solutions with known concentrations were spiked into the actual samples to calculate the recovery rate for further verification of the accuracy and precision of the proposed sensor (Table 2). The recovery rates of DA and UA are in the range of 91.4 ~ 98.0% and 93.1 ~ 105.4%, respectively. It is worth noting that when using real samples, the shape and position of the DPV curve will not be affected. These results confirm that biological matrices such as human serum do not affect the simultaneous determination of DA and UA.

Table 2 Detection results of DA and UA in human serum samples using GNPs@CDs/erGO/GCE.

Sample	**Analyte**	**Detected (μM)**	**Added (μM)**	**Measured (μM)**	**Recovery (%)**
sample 1	DA	–	1.00	0.93	93.0
			5.00	4.57	91.4
	UA	0.71	1.00	1.64	93.0
			5.00	5.98	105.4
sample 2	DA	–	1.00	0.98	98.0
			5.00	4.81	96.2
	UA	0.98	1.00	1.94	96.0
			5.00	6.24	105.2

4. CONCLUSIONS

In summary, an ultrasensitive electrochemical sensing platform based on the GNPs@CDs nanoparticles combined with erGO was successfully constructed and employed for simultaneous determination of DA and UA. The modified electrode exhibited excellent electrocatalytic properties toward oxidation of DA and UA in the presence of AA with well-separated peak potentials, increased current responses, low detection limits (3.1 nM of DA and 33.5 nM of UA), highly sensitivity, long-term stability, good reproducibility, and favorable recoveries in practical sample analysis.

ACKNOWLEDGMENTS

This work was financially supported by the National Natural Science Foundation of China (Nos. 32072334, 31672457), the Natural Science Foundation of Hunan Province, China (2020JJ4035), the Foundation of Hunan Provincial Key Laboratory of Crop Germplasm Innovation and Resource Utilization (18KFXM07), Hunan Provincial Science and Technology Department (2018WK4025, 2020NK2004, 2020ZL2004), and double first-class construction project of Hunan Agricultural University (SYL201802003, YB2018007, CX20190497).

SUPPLEMENTARY MATERIAL

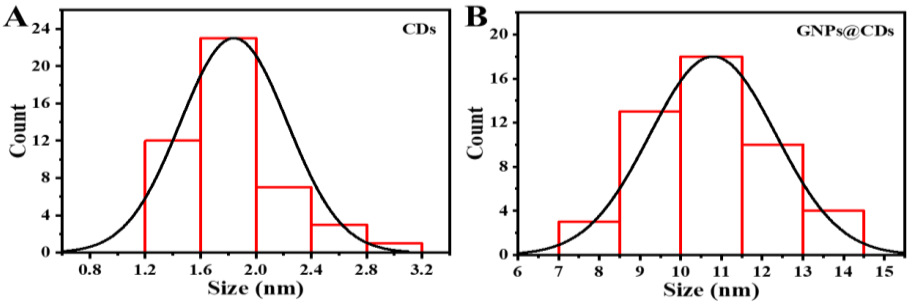

Figure S1. The particle size distribution of CDs (A) and GNPs@CDs (B).

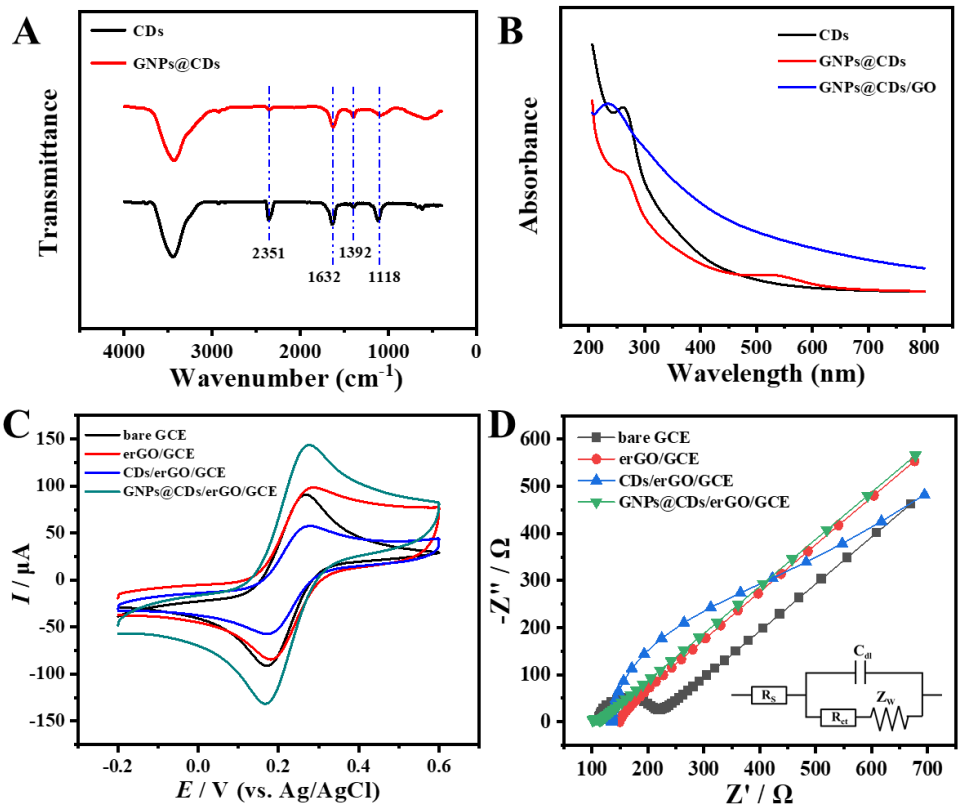

Figure S2. (A) IR transmission spectra of CDs and GNPs@CDs. (B) UV-vis spectra of CDs, GNPs@CDs, and GNPs@CDs/GO. (C) CV current responses of differently modified electrodes in 5 mM $[Fe(CN)_6]^{3-/4-}$ (1:1) in 0.1 M KCl. (D) Nyquist plots of different electrodes for the EIS measurements in the presence of 5 mM $[Fe(CN)_6]^{3-/4-}$ (1:1) in 0.1 M KCl.

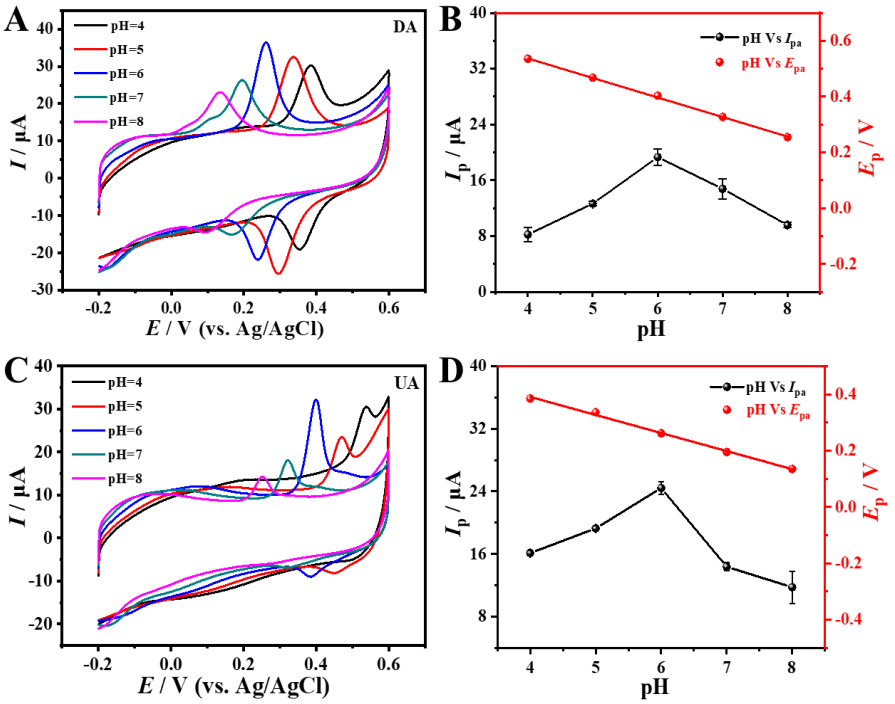

Figure S3. Cyclic voltammograms of 5 μM DA (A) and 5 μM UA (C) recorded at different pH from 4 to 8. Linear plots of the anodic peak potential of DA (B) and UA (D) against pH and effect of pH on the response anodic peak current at a scan rate of 50 mV s^{-1}.

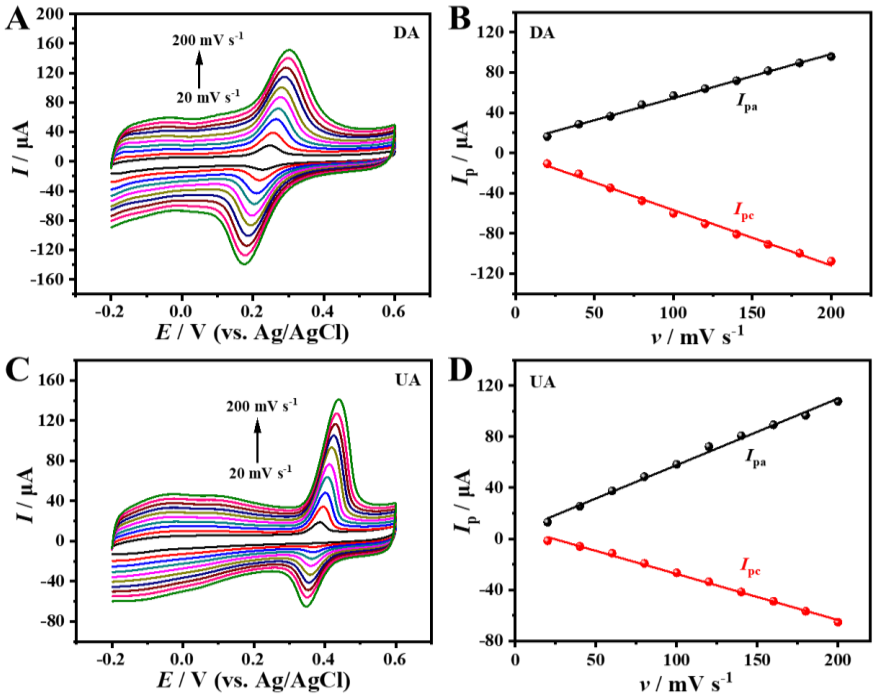

Figure S4. The effect of voltammetric scan rates on the redox peak currents of (A) 20 μM DA and (B) 20 μM UA with GNPs@CDs/erGO/GCE in 0.2M PBS (pH 6.0) and linear relationship between peak currents and the scan rate (v) of DA (C) and UA (D).

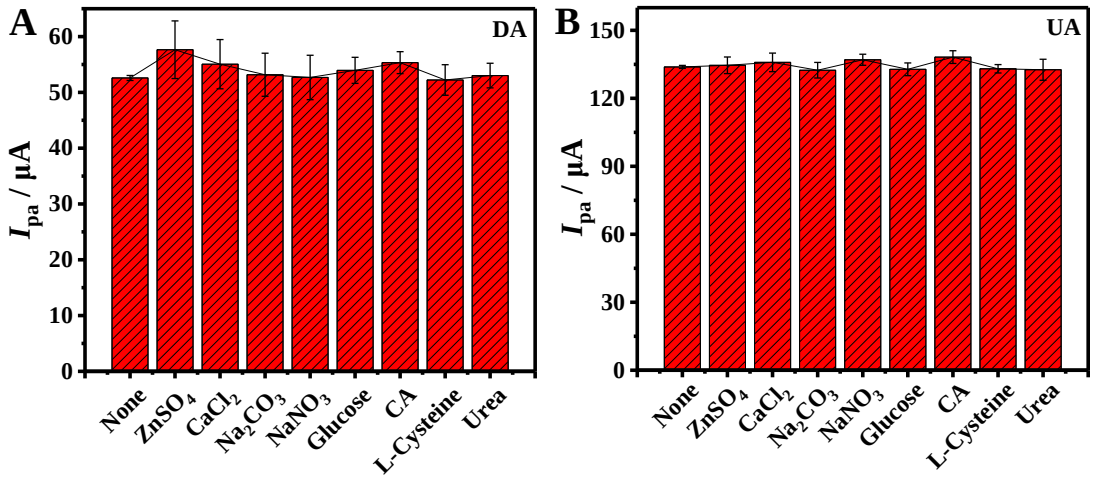

Figure S5. Degree of inhibition of DA (A) and UA (B) with GNPs@CDs/erGO/GCE in the presence of various potentially interfering species.

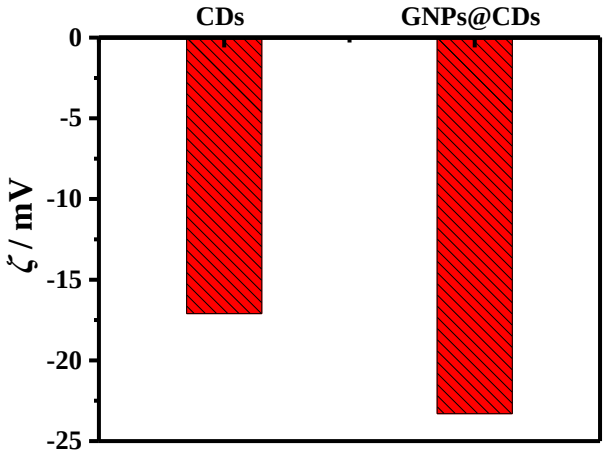

Figure S6. Zeta potential of CDs and GNPs@CDs.

Table S1. The changes of binding energy peak areas of CDs before and after reduction.

Binding Energy	Area (CPS. eV)		Area Ratio	
(eV)	CDs	GNPs@CDs	CDs	GNPs@CDs
284.6 (C-C)	29259.85	25032.4	1.0	1.0
286.0 (C-OH)	6996.28	10317.26	0.26	0.49
287.7 (C=O)	3307.86	4152.45	0.1	0.25
289.0 (COOH)	934.58	2037.21	0.02	0.12

References

1. J. M. Zen and P. J. Chen, *Anal. Chem.*, 69 (1997) 5087.
2. J. Ping, J. Wu, Y. Wang and Y. Ying, *Biosens. Bioelectron.*, 34 (2012) 70.
3. L. W. Zhao, H. J. Li, S. M. Gao, M.J Li, S. Xu, C.P Li, W.L Guo, C.Q. Qu and B.H Yang, *Electrochim. Acta*, 168 (2015) 191.
4. X. Ren, T. Zhang, D. Wu, T. Yan, X. Pang, B. Du, W. Lou and Q. Wei, *Biosens. Bioelectron.*, 94 (2017) 694.
5. S. Zhou, H. Shi, F. Xun, K. Xue, W. Song, *Biosens. Bioelectron.*, 42(2013) 163.
6. A. K. Geim, *Science*, 324 (2009) 1530.
7. X. Xu, R. Ray, Y. Gu, H.J. Ploehn, L. Gearheart, K. Raker, Walter A, *J. Am. Chem. Soc.*, 126 (2004) 12736.
8. S. Stankovich, D.A. Dikin, R.D. Piner, K.A. Kohlhaas, A. Kleinhammes, Y. Jia, W. Yue，S.B.T. Nguyen and R.S Ruoff, *Carbon*, 45 (2007) 1558.
9. P.G. Su and L.Y. Yang, *Sens. Actuators B Chem.*, 223 (2016) 202.
10. H.Y. Wei, T.Y. Huang and C.W. Kung, *J. Mater. Chem. A*, 2(2014) 7229.
11. R.G. Bai, K. Muthoosamy, F.N. Shipton, A. Pandikumar, P. Rameshkumar, N.M. Huang and S. Manickam. *RSC adv.*, 6(2016) 36576.
12. Y. Li, T. Wen, C. Xue, Q. Han, Y. Wang, J. Hong and H. Jiang, *Biosens. Bioelectron.*, 42(2013) 287.
13. L. Zhang, Y. Han, J. Zhu, Y. Zhai and S Dong, *Anal. Chem.*, 87(2015) 2033.
14. K. Li, J. Xu, M. Arsalan, N. Cheng, Q. Sheng, J. Zheng, C, Wei, T Yue, *J. Electrochem. Soc.*, 166 (2019) B56.
15. Y.P. Sun, B. Zhou, Y. Lin, W. Wang, K.A.S. Fernando, P. Pathak, M.J. Meziani, B.A. Harruff, X. Wang and H Wang, *J. Am. Chem. Soc.*, 128 (2006) 7756.
16. J. Deng, Q. Lu, N. Mi, H. Li, M. Liu, M. Xu, L. Tan, Q. Xie, Y Zhang and S. Yao, *Chemistry*, 20 (2014) 4993.
17. X. Wang, Y. Long, Q. Wang, H. Zhang, X. Huang, R. Zhu, P. Teng, L. Liang, H. Zheng, *Carbon*, 64(2013) 499.
18. R. Paul, L. Zhu, H. Chen, J. Qu and L. Dai, *Adv. Mater.*, 31 (2019) e1806403.
19. P.D. Nellist and S.J. Pennycook, *Ultramicroscopy*, 78 (1999) 111.
20. Z. Zhong, J. Ho, J. Teo, S. Shen and A. Gedanken, *Chem. Mater.*, 19 (2007) 4776.
21. Z. Cai, Y. Ye, X. Wan, J Liu and Q. He, *Nanomaterials*, 9 (2019) 835.
22. Q. He, J. Liu, X. Liu, G. Li, D. Chen, P. Deng and J. Liang, *Electrochim. Acta*, 296 (2019) 683.
23. Q. He, J. Liu, X. Liu, G. Li, P. Deng and J. Liang, *Colloids Surf. B*, 172 (2018) 565.
24. G. Li, S. Wang and Y.Y. Duan, *Sens. Actuators B Chem.*, 277 (2018) 250.
25. G. Li, S. Wang and Y. Y. Duan, *Sens. Actuators B Chem.,* 241 (2017) 1244.
26. G. Li, Z. Dan, S. Wang and Y. Y. Duan, *Sens. Actuators B Chem.*, 237 (2016) 167.
27. K. Zhang, X. Chen, Z. Li, Y. Wang, S. Sun, L. Wang, T. Guo, D. Zhang, Z. Xue and X. Zhou, *Talanta*, 178 (2018) 315.
28. J. Li, J. Yang, Z. Yang, Y. Li, S. Yu, Q. Xu and X. Hu, *Anal. Methods*, 4 (2012) 1725.
29. X. Chen, D. Li, W. Ma, T. Yang and D. Zhang, *Microchim. Acta*, 186 (2019) 407.
30. J. Feng, Q. Li, J. Cai, T. Yang and Junhong, *Sens. Actuators B Chem.*, 298 (2019) 126872.
31. M.M.A.E. Nusiba, J. Abdullah, S. Kamaruzaman, M.I. Saiman and Y. Sulaiman, *Arabian J. Chem.*, 11 (2018) 1301.
32. A. Mehta, D. Pooja, A. Thakur and S. Basu, *New J. Chem.*, 41 (2017) 4573.
33. J. Ju and W. Chen, *Anal. Chem.*, 87 (2015) 1903.
34. S. He, P. He, X. Zhang, X. Zhang, K. Liu, L. Jia and F. Dong, *Anal. Chim. Acta,* 1031 (2018) 75.
35. J. Chen, P. He, H. Bai, S. He, T. Zhang, X. Zhang and F. Dong, *Sens. Actuators B Chem.*, 252(2017) 9.
36. J. Wang, B. Yang, J. Zhong, B. Yan, K. Zhang, C. Zhai, Y. Shiraishi, Y. Du and P. Yang, *J. Colloid*

Interface Sci., 497 (2017) 172.
37. G. Valenti, E. Rampazzo, S. Kesarkar, D. Genovese, A. Fiorani, A. Zanut, F. Palomba, M. Marcaccio, F. Paolucci and L. Prodi, *Coord. Chem. Rev.*, 367 (2018) 65.
38. H.S. Jang, D. Kim, C. Lee, B. Yan, X. Qin and Y. Piao, *Inorg. Chem. Commun.*, 105 (2019) 174.
39. E. Priyadarshini, K. Rawat, T. Prasad and H.B. Bohidar, *Colloids Surf. B*, 163 (2018) 355.
40. T.J. Macdonald, K. Wu, S.K. Sehmi, S. Noimark, W.J. Peveler, H.D. Toit, N.H. Voelcker, E. Allan, A.J. Macrobert and A. Gavriilidis, *Sci. Rep.*, 6(2016) 39272.
41. H. You, Z. Mu, M. Zhao, J. Zhou, Y. Chen and L. Bai, *Microchim. Acta*, 186(2019) 12.
42. X. Chen, G. Zhang, Y. He, L. Shi, J. Zhang, G. Yang, H. Pan, W. Liu and S. Feng, *Int. J. Electrochem. Sci.*, 15 (2020) 5927.
43. L. Shi, Z. Wang, X. Chen, G. Yang and W. Liu, *Int. J. Electrochem. Sci.*, 14 (2019) 8882.